

Figure 2.1.1: (color online) Schematic representation of: **elastic** a (population of the ground state), and **inelastic** b (population lowest octupole vibration at 2.62 MeV) processes associated with the reaction  $^{208}\text{Pb}(\alpha, \alpha')^{208}\text{Pb}^*$  (for more details see Sect. 2.3 and App. 2.A). In the inset (I) a schematic Nuclear Field Theory (reaction plus structure) (NFT(r+s)) diagram describing the elastic process (potential scattering, dashed horizontal line) is displayed (see e.g. Broglia et al. (2016) and refs. therein). The  $\alpha$ -projectile moving in the continuum is represented by an arrowed (curved) line. From the measurement of the elastic differential cross section one can deduce the partial wave phase shifts (Appendix 2.C). In the inset (II) a schematic NFT(r+s) diagram describing the inelastic excitation (see Fig. 2.C.1) of the low-lying octupole vibration (wavy line) of  $^{208}\text{Pb}$  by the action of the transient field created by the  $\alpha$ -particle on the target (horizontal dashed line) is given (see App. 2.A). Outgoing  $\alpha$  particles are deflected in a spectograph and recorded in a detector. The corresponding excitation function is given in the lowest part of the figure (after Mottelson (1976b)).

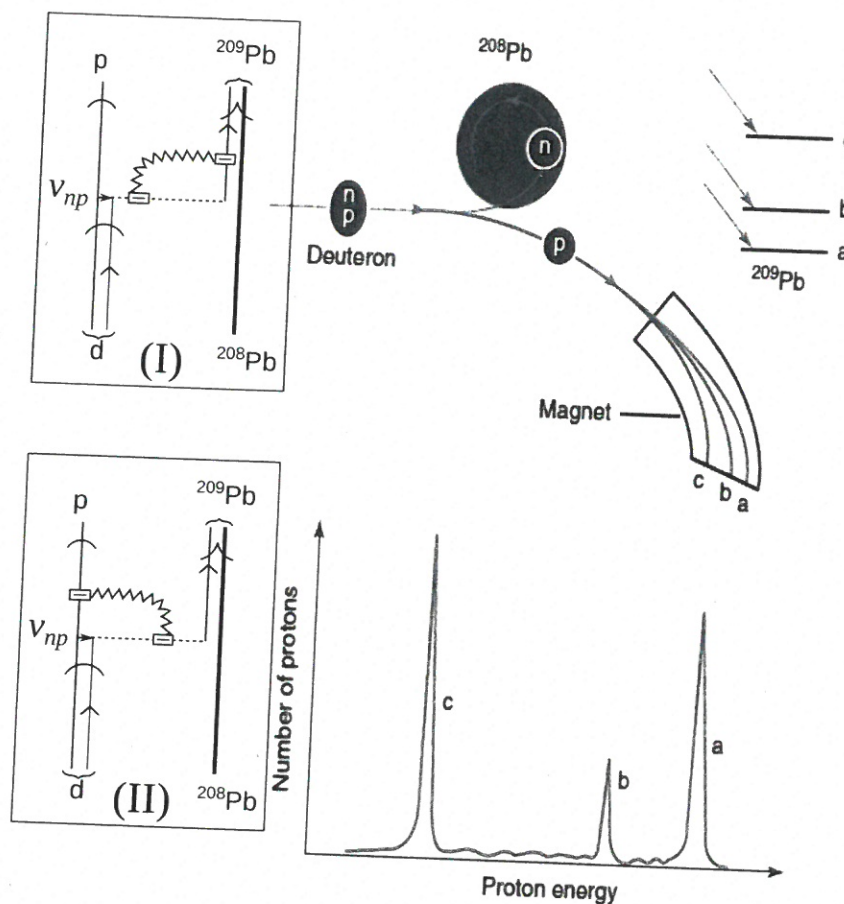


Figure 2.1.2: (Color online) Schematic representation of the one-nucleon transfer reaction  $^{208}\text{Pb}(d, p)^{209}\text{Pb}$  populating valence single-particle states of  $^{209}\text{Pb}$ . In the inset a schematic NFT(r+s) diagram describing the process is shown. Curved arrowed lines describe the projectile  $d$  (deuteron) and outgoing particle  $p$  (proton) moving in the continuum. The short horizontal arrowed line labeled  $v_{np}$  represents the proton-neutron interaction inducing the transfer process (dashed horizontal line) while the open dashed rectangle indicates the Particle Recoil Coupling (PRC) vertex. That is, the coupling of the relative motion to the recoil process described in terms of a jagged line (App. 2.C). This information is carried out in the center of mass system by the outgoing particles in the final channel. Within this context the jagged line is involved in a virtual process (insets (I) and (II)). The energy and momentum of the outgoing proton reflects the recoil, the  $Q$ -value of the reaction and the excitation energy of the final state as analyzed in the magnet and recorded in the particle detector (a,b,c) (after Mottelson (1976b)).

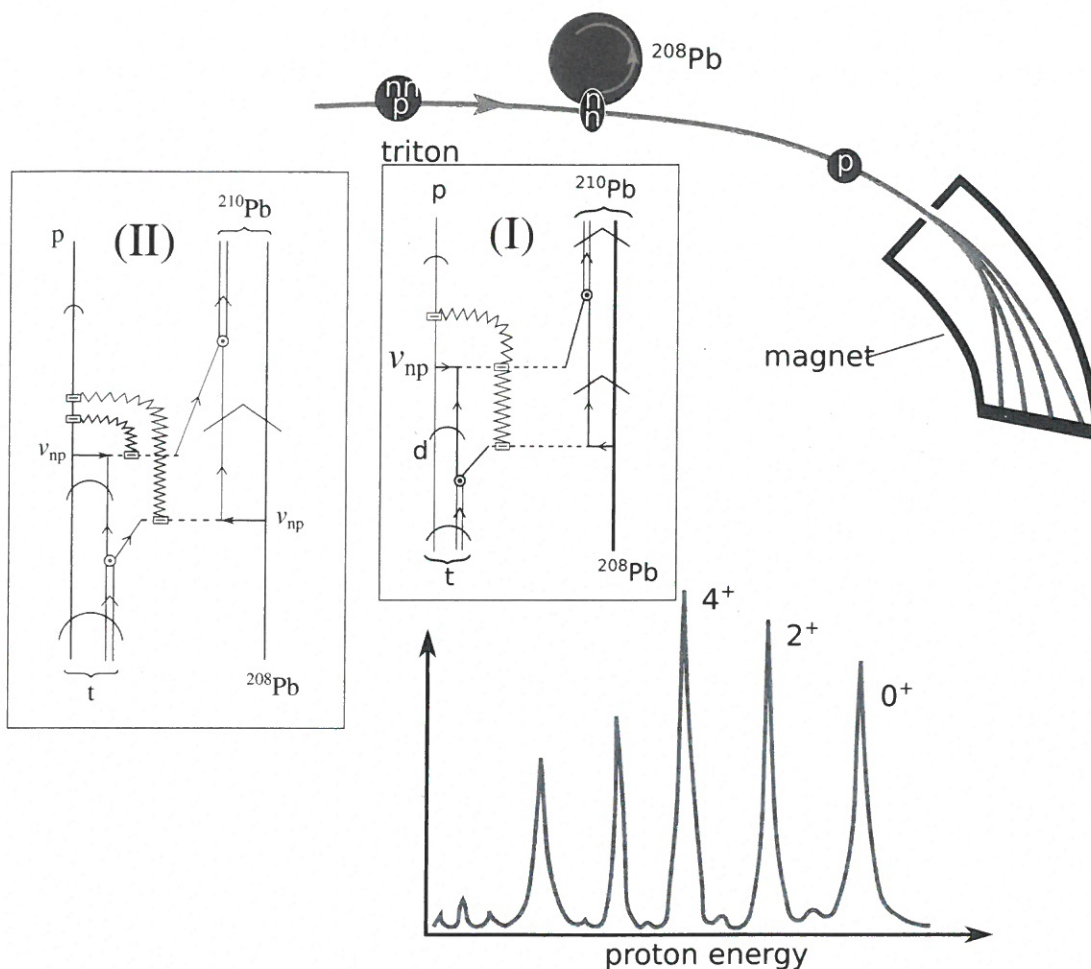


Figure 2.1.3: (Color online) Schematic representation of the two-nucleon transfer reaction  $^{208}\text{Pb}(t, p)^{210}\text{Pb}$  process populating the ground state  $0^+$ , and two particle excited states  $2^+$  and  $4^+$ . That is, monopole, quadrupole and hexadecapole pair addition modes (multipole pairing vibrations) of  $^{208}\text{Pb}$  (App. 7.F; see also Brink, D. and Broglia (2005) Sect. 5.3.1 p. 108). In the inset (I) a NFT( $r+s$ ) diagram of the (successive) transfer process is displayed. The jagged line brings information to the outgoing nuclei in the exit channel (CM system), of the change in scaling in the asymptotic outgoing waves with respect to the incoming ones, concerning the different mass partitions (recoil) of summed value  $2m$  (App. 2.C; concerning the apparent non-linearity that is the direct coupling of two recoil modes, this can be avoided drawing the process as shown in inset (II); see also Sect. 2.B.3; see also Fig. 2.7.10), this information is carried out to the detector by the outgoing proton (see App. 2.B, Sect. 2.B.3) (after Mottelson (1976b)).

one calls a physically (clothed) particle is only partially to be associated with that particle field alone. It is also partially to be associated with the vibrational fields (surface, density, spin<sup>24</sup>, pairing<sup>25</sup>, etc. vibrational modes), because they are in interaction through the particle-vibration coupling vertices<sup>26</sup>. And conversely, what one calls a nuclear vibration can couple to particle-hole (in the case of a surface vibration), two-particle (in the case of a pair addition) or a two-hole (in the case of a pair removal) configurations.

Thus nucleons (fermions) couple to vibrational modes (bosons) and, eventually, can reabsorb them returning to the original state. The same is true concerning bosons degrees of freedom and their coupling to fermions. The outcome of such processes, namely the dressed physical elementary modes of excitation, is closely connected with the renormalization program of quantum electrodynamics (QED)<sup>27</sup> implemented in NFT in terms of Feynman diagrams. Renormalized NFT, i.e (NFT)<sub>ren</sub> implies that the intermediate, virtual states clothing the elementary modes of excitation, are fully dressed<sup>28</sup>.

The specific experimental probes of the bare elementary modes of nuclear excitation reveal only one aspect, in most cases likely the most important one of the physical (clothed) elementary modes. Renormalized NFT reflects the physical unity of low-energy nuclear research requiring the melting not only of elementary modes of excitation but also of structure and reaction theory, let alone of the different experimental techniques developed to study the atomic nucleus. In other words the need for a complete set of experimental probes to reveal the multi faceted properties of clothed elementary modes of excitation resulting from the implementation of a consistent program of structure and reactions (within this context see Fig. 2.10.1).

As seen from the contents of the present monograph, the accent is set at relating theoretical predictions with experimental findings, through the unification of structure and reactions. In particular the unification of pairing and two-nucleon transfer processes, where the two subjects are blended together, which is what happens in nature. Once the NFT rules to work out the variety of elements (spectroscopic and, with the help of them, reaction amplitudes) have been laid out and/or the pertinent literature refer to, concrete embodiments are provided and eventual absolute cross sections and transition probabilities calculated and confronted with the experimental data.

An essential test theory has to pass is particle-pair conservation. Test closely connected with some operator identities which go under the name of sum rules. An overcomplete basis of states will violate sum rules, resulting in couplings between the basis states. Couplings which are proportional to the overlap (non-orthogonality) between these states. This is so, not only for structure calculations,

<sup>24</sup>Bertsch and Broglia (2005) Chs. 6,7,8.

<sup>25</sup>Brink, D. and Broglia (2005) Ch. 5.

<sup>26</sup>Bohr, A. and Mottelson (1975).

<sup>27</sup>Feynman (1975); Schwinger (2001).

<sup>28</sup>Barranco et al. (2017), see also Broglia et al. (2016).

replace by (T-F) p. 67 handwritten

to p. 67

København 20/2/2020

(67)

(T) An essential test theory has to pass is particles as well as pair conservation. Such a test is, in the first case, closely connected in the first case with some operator identities which are known as sum rules\*. An overcomplete (non-orthogonal) set of basis states, like that provide by an elementary mode of excitation, will violate sum rules. As we shall see, taking into account the couplings between these modes following the rules of NFT (see Sect. 2.7) eliminates such violations.

For example, a hole and a pair addition is non-orthogonal to a particle and a surface (p.h.) vibration (Sect. 2.5; also 2.7.4)

A similar situation is found in the case of e.g. two-nucleon transfer, because the single-particle states in projectile and target are, as a rule, non-orthogonal. Taking into account such overlaps one can remove the overcounting (see Secs. 4.2, 6.2, 9 and App. 6.c)

(T)

to p. 67

\* See e.g. Bertsch and Broglia (2005) ch. 4, Bortignon et al, chs. 3 and 8 and refs. therein.

(1998)

in which e.g. hole and pair addition modes are non orthogonal to particle and surface ( $p, h$ ) vibrational states. Also for reactions calculations, as the single-particle states in projectile and target are, as a rule, non orthogonal. Sum rules play a central role not only in the validation of a theory, but also in defining the variety of couplings which dress the bare basis states as well as to eliminate spurious components from reaction amplitudes.

## 2.2 Sum rules

A quantitative measure of the overcompleteness of the elementary modes of excitation basis is provided by the use of exact and of empirical sum rules that the observables (cross sections) associated with the variety of probes to which the nucleus is subject, have to fulfill. An example of the first type is given by the Thomas-Reiche-Kuhn (TRK) sum rule<sup>29,30</sup>, while of the second type, by some of the two-nucleon transfer reaction (TNTR) sum rules<sup>31</sup>. Others, which relate one-with two-particle transfer processes<sup>32</sup> being exact. In all cases they embody particle (pair) number conservation. Charged particles in the first case (electrons in atoms and molecules, effective charges of neutrons and protons in nuclei). Number of Cooper pairs in nuclei in the second<sup>33</sup>. Physically, they provide information concerning: 1) the maximum amount of energy which the quantal system can absorb from a beam of photons ( $\gamma$ -rays) shined on it; 2) the total two-nucleon transfer cross section (ring area fraction of the geometrical reaction cross section) exhausted by the final ( $A \pm 2$ ) states populated in the transfer process.

In other words, these sum rules provide a quantitative measure of the single-particle subspace the quantal system under study, in particular the nucleus, uses to correlate particle-hole excitations and thus induce the antenna-like motion of protons against neutrons or, to correlate pairs of nucleons moving in time reversal states around the Fermi energy, leading to a, static or dynamic, sigmoidal distribution of the associated pair ( $v, \bar{v}$ ) level occupancy around the Fermi energy.

The TRK sum rule can, in the nuclear case, be written as<sup>34</sup>

$$S(E1) = \sum_{\alpha} |\langle \alpha | F | \tilde{0} \rangle|^2 (E_{\alpha} - E_0) = \frac{9}{4\pi} \frac{\hbar^2 e^2}{2m} \frac{NZ}{A}, \quad (2.2.1)$$

<sup>29</sup>Bohr, A. and Mottelson (1975), Sect. 6-4.

<sup>30</sup>Bertsch and Broglia (2005), Chapter 3, in particular Sect. 3.3.

<sup>31</sup>Broglia, R. A. et al. (1972)

<sup>32</sup>Bayman, B. F. and Clement (1972); Lanford (1977)

<sup>33</sup>Within this context, the absolute two-nucleon transfer cross section populating the ground state of a superfluid nucleus is proportional to the number of Cooper pairs contributing to the nuclear condensate (modulus squared). This quantity is rather stable along a pairing rotational band, in keeping with the fact that the “intrinsic”  $|BCS\rangle$ -state of the deformed system in gauge space, is essentially the same for all members of the band. This fact is at the basis of a newly found physical sum rule (Potel et al. (2017); see also Ch. 7 Sect. 7.4.1).

<sup>34</sup>Bohr, A. and Mottelson (1975); Bertsch and Broglia (2005); Bortignon, P. F. et al. (1998)

while all the RPA solutions are included in the intermediate states. The quadrupole surface vibrational modes were allowed only as intermediate states. The single hole and particle states  $j_1^{-1}$  and  $j_2$ , respectively, correspond to experimentally known levels around the  $Z = 82$  shell closure. In what follows, the two  $\frac{3}{2}^+$  states built out of the  $|d_{3/2}^{-1} \otimes gs(^{210}\text{Po})\rangle$  and  $|h_{9/2} \otimes 3^-(^{208}\text{Pb})\rangle$  configurations are studied in this space. This two-state system provides a rich laboratory to learn about the interplay of surface and pairing modes.

The two basis states

$$|\alpha\rangle \equiv |d_{3/2}^{-1} \otimes gs(^{210}\text{Po}); 3/2^+\rangle \quad (2.7.92)$$

and<sup>113</sup>

$$\text{single-particle} \quad |\beta\rangle \equiv |h_{9/2} \otimes 3^-(^{208}\text{Pb}); 3/2^+\rangle \quad (2.7.93)$$

are 118 keV apart. They mix strongly through the couplings depicted by the graphs a) and b) of Fig. 2.7.11.

Because of the energy dependence of  $h_{eff}$  there is a different matrix element for each final state. The diagonalization of the matrices was carried out self-consistently, *i.e.* the energy denominators of the different graphs are to be calculated by utilizing the exact energies<sup>114</sup>. The corresponding graphical contributions to the spectroscopic factor and inelastic cross-sections are also collected in fig. 2.7.11. To be noted is the very different ratio of the  $(d, d')$  and  $(t, \alpha)$  cross sections. While  $R_1 = B(E3; (\frac{3}{2})_1)/B(E3; (\frac{3}{2})_2)$  is approximately equal to 2.5, the ratio  $R_2 = \sigma((t, \alpha); (\frac{3}{2})_2)/\sigma((t, \alpha); (\frac{3}{2})_1)$  is close to one. Because the component  $|\beta\rangle$  carries the inelastic-scattering strength, while the  $(t, \alpha)$  reaction proceeds mainly through the component of type  $|\alpha\rangle$ , the difference between  $R_1$  and  $R_2$  can be traced back to the corrections associated with the over-completeness of the unperturbed basis states which give rise to rather different normalizations of the two physical states (see Sects. 2.5 and 2.7.3, see also App. 2.B, Sect. 2.B.2).

## 2.8 Competition between the variety of ZPF, in particular those associated with density ( $\beta = 0$ ) and pairing ( $\beta = \pm 2$ )

Particle-hole like vibrations, as e.g. collective surface quadrupole vibrations, induce dynamical distortions of the mean field which virtually break the magnetic degeneracy of levels into two-fold (Kramer's) degenerate (Nilsson-like) levels and to a reduction of the size of the discontinuity at the Fermi surface typical of non-interacting Fermi systems. Pairing vibrations also smooth out the sharp discontinuity of occupancy taking place around the Fermi energy displayed by closed shell

<sup>113</sup>Although not likely, the reader is advised not to confuse the label of the state  $|\beta\rangle$  with the transfer quantum number  $\beta$  used above.

<sup>114</sup>for more details, see ref. Bortignon, P. F. et al. (1977); see also Bortignon et al. (1976).

absolute  
( $t, \alpha$ ) differ-  
ential cross  
sections,

italics

b - b  
from  
127a -

127c

(b) to p. 127

Elementary modes of excitation and specific probes

The picture of nuclear structure achieved in terms of elementary modes of excitation displays in a transparent manner the correlation aspects of nuclear dynamics. And, as a consequence or better as a result of the physical input at the basis of the picture, it points to the reaction process specific to bring the structure information to the detector (observer).

The wavefunctions resulting from the NFT solution of the finite quantal nuclear many-body problem contain only few components. Each of them make direct reference to a specific probe. In particular inelastic scattering and one- and two-particle transfer reactions. That is, each component is related to an observable, and is thus associated with a concrete experiment one knows how to carry out with the help of accelerators, beams (in e.g. inverse kinematics), targets (active or less), detectors and softwares, whose output directly relate to the observer. Said it differently, the elementary modes of excitation picture calls for a unified nuclear field theory description of structure and reactions (see also Sect. 7.6.2). More precisely, to the question concerning how the nuclear structure of the one-proton outside closed shell nucleus  $^{209}_{83}\text{Bi}$  is, a possible answer reads as following: a subtle interplay between the vacuum state, that is the ground state of the double closed

Kobberlarn 7/10/20  
927b

shell nucleus  $^{208}_{82}\text{Pb}_{126}$ , its first excited collective state  $|3^-(^{208}\text{Pb}); 2,613 \text{ MeV}\rangle$  and the proton pair addition mode  $1g_8 (^{210}_{84}\text{Po}_{126})\rangle$  as far as boson elementary modes of excitation with  $\beta=0$  and  $\beta=+2$  transfer quantum number is concerned, and a one-proton ( $\beta=+1$ ) and one-proton hole ( $\beta=-1$ ) above and in the  $Z=82, N=126$  vacuum state respectively, concerning the fermion degree of freedom. Consistent with this scenario, inelastic scattering and Coulomb excitation ( $^{209}\text{Bi}(d, d')$  and  $^{209}\text{Bi}(d, \alpha')$  respectively), and one-proton stripping and pickup reactions ( $^{208}\text{Pb}({^3}\text{He}, n) ^{209}\text{Bi}$  and  $^{210}\text{Po}(t, d) ^{209}\text{Bi}$  respectively) together with two-proton stripping processes (e.g.  $^{207}\text{Tl}({^3}\text{He}, n) ^{209}\text{Bi}$ , possible only in inverse kinematics), are the specific experimental probes.

The need to include both single-particle and collective modes to describe the elementary excitations (reactions) of nuclei subject to external probes, implies that one employs an overcomplete (non-orthogonal) set of variables.

From the existence of the nuclear shell structure, interactions can be regime

this is a nuclear  
Han (1.2.8) p.122

[S-matrix p.515]

rented in first approximation by an average field. Thus one can describe the coupling between single-particle and collective vibrations by a three-point (-field) vertex (Fig. 2.7.4) rather than a four-point (-field) vertex representing the bare nuclear interaction (Fig. 2.2.1(a)). It is of notice that according to rule II of NFT, this interaction is to be considered in working out the different diagrams (see also (1.2.8)).

Concerning the role of non-orthogonality between elementary modes of excitation we also refer to two-nucleon transfer processes (Fig. 4.1.2, as well as App. 6.C), in which case, simultaneous transfer is partially mediated by the finite overlaps of the single-particle wavefunctions in target and projectile, contribution which is to be eliminated from the total transition amplitudes. A similar requirement is found at the basis of the derivation of the tunneling Hamiltonian associated with weakly coupled superconductors (Josephson junction, sect. 4.6).

(b)  
top 127

## 2.9. OPTICAL POTENTIAL AND TRANSFER

*Coupling between structure and reaction*

131

### 2.9 Optical potential and transfer channels

In this Section the unification of NFT of structure and reactions is further developed using as example the light exotic two-neutron halo nucleus  $^{11}\text{Li}$ . In particular, we dwell upon the variety of renormalization processes and associated form factors needed to calculate one- and two- neutron transfer reactions. The use of the same elements in the eventual calculation of the polarization contribution to the optical potential, ~~is also discussed a subject not treated in the present monograph, is briefly mentioned below.~~ corresponding

#### 2.9.1 Bare particles and Hartree-Fock field

Nucleon elastic scattering experiments at energies of tens of MeV can be accurately described in terms of an optical potential in which the real component is parametrized according to the (Woods-Saxon) potential<sup>118</sup>,

$$U(r) = U f(r), \quad (2.9.1)$$

$f(r)$  being a Fermi (sigmoidal) function, of radius  $R_0 = r_0 A^{1/3}$  ( $r_0 = 1.2$  fm), diffusivity  $a = 0.65$  fm, and strength

$$U = U_0 + 0.4E \quad (2.9.2)$$

where

$$U_0 = V_0 + 30 \frac{N - Z}{A} \text{ MeV}, \quad V_0 = -51 \text{ MeV}, \quad (2.9.3)$$

while  $E$  is the energy of the scattered particle  $\epsilon_k = \hbar^2 k^2 / 2m$ , measured from the Fermi energy,  $m$  being the nucleon mass. In the case of  $^9\text{Li}_6$ ,  $U_0 \approx -41$  MeV. One can replace the  $k$ -dependence in (2.9.2) by the so-called  $k$ -mass<sup>119</sup>

$$m_k = m \left( 1 + \frac{m}{\hbar^2 k} \frac{dU}{dk} \right)^{-1}, \quad (2.9.4)$$

where the energy independent Woods-Saxon potential has a depth given by  $\left(\frac{m}{m_k}\right) U_0 = U'_0$ <sup>120</sup>. For the nucleons of the core, i.e. of  $^9\text{Li}$ ,  $m_k = m(1 + 0.4)^{-1} \approx 0.7m$ . For the halo neutrons<sup>121</sup>,  $m_k/m = (1 + O \times 0.4)^{-1}$ , where  $O (= (R_0/R)^3)$  is the overlap between the core and the halo nucleons. Making use of the values  $R_0 = 2.66$  fm and  $R = 4.58$  fm (see Eq. 4.C.4) one obtains  $O \approx 0.2$  (see (3.6.8)) and thus,  $m_k \approx 0.93m$ .

<sup>118</sup>cf. e.g. Bohr and Mottelson (1969) and refs. therein.

<sup>119</sup>What in nuclear matter is called the  $k$ -mass and is a well defined quantity, in finite systems like the atomic nucleus, in which linear momentum is not a conserved quantity, is introduced to provide a measure of the spatial non-locality of the mean field, and is defined for each state as the expectation value of the quantity inside the parenthesis in Eq. (2.9.4), calculated making use of the corresponding single-particle wavefunction (see e.g. ref. Bernard and Giai (1981), in which case  $m_k$  is referred to as the non-locality effective mass)

<sup>120</sup>See e.g. Fig. 2.14 Mahaux, C. et al. (1985).

<sup>121</sup>Assuming a velocity independent  $v$ , the  $k$ -dependence of the mean field stems from the exchange (Fock) potential  $U_x(\mathbf{r}, \mathbf{r}') = - \sum_i \varphi_i^*(\mathbf{r}') v(|\mathbf{r} - \mathbf{r}'|) \varphi_i(\mathbf{r})$  (linear in  $O$ ), while the central potential

\* (M) - (M) handwritten Jr. 131a

(M) \*) There exists a vast literature concerning this subject. a  
See e.g. Feshbach(1958), Feshbach Reaction Theory( ),  
R. Gatchler (1983), D. F. Jackson <sup>(N. Austern (1970))</sup>, Dickhoff  
and Van Nech (2005), Dickhoff, Charity and Mahzoon,  
(2017), R. Sartor and C. Mahaux P.R. 21C (1980) 2613,  
J.P. Jeuhenne and C. Mahaux, Nucl. Phys. A136 (1969) 149  
C. Mahaux Ann. Rev. Nucl. Sci. 23, 193 (1973),  
Jeuhenne, Lejenne, C. Mahaux Phys. Rev. 25C, 83 (1976),  
G. Pollaro, Broglia, Winter NPA 406, 369 (1983),  
Broglia + Winter (2004), and refs. therein

gregory agrega otras referencias  
al potential optico que tu conoscas.

p. 131

(M)

Montanari, Arradi, etc  
PRL

interaction making it subcritical, ii) to screen the (repulsive) symmetry interaction, and (consequently), iii) to allow the presence at low energies of a consistent fraction of the TRK-sum rule associated with the GDR at  $\approx 36$  MeV. In fact, a  $1^-$  resonance carrying  $\approx 8\%$  of the TRK sum rule and with centroid at an energy  $\lesssim 1$  MeV have been observed<sup>127</sup>. Thus, the connotation of pygmy dipole resonance (PDR)<sup>128</sup>. Exchanged between the heavily dressed neutrons moving in parity inverted states provides, together with the contribution of the strongly screened, bare  $NN$ -pairing interaction, the glue needed to bind the neutron halo Cooper pair to the  $^9\text{Li}$  core. With some experimental input<sup>129</sup>, NFT allows to, accurately and economically, propagate dressing effects which not only renormalizes mean field, but overwhelms it providing an overall account of the experimental findings. The many-body effects at the basis of these phenomena are carried out in three steps, as schematically displayed in Fig. 2.9.1 and described below. For details see Sect.

3.6)<sup>130</sup>:

*bold*

1) Starting with well defined elements: Woods-Saxon (WS) potential, and the parameters characterizing the low-lying quadrupole vibration of the core  $^9\text{Li}$  (**input**, double boxed quantities), calculate the single-particle levels and collective vibration (separable interaction) and determine the corresponding particle-vibration coupling vertices (strength and form factors). From the ratio of the WS radius ( $R_0$ ) and of the observed one ( $R^{(11\text{Li})}$  **input**) determine the overlap  $O$ . Because  $O \ll 1$ , the contribution of the exchange (Fock) potential to the empirical WS potential is small concerning the halo neutrons<sup>131</sup>. Consequently the neutron halo  $k$ -mass  $m_k$  has a value close to the bare mass  $m$ .

*bold*

2) Making use of the above elements one can cloth the bare single-particle states, in particular the  $s_{1/2}$  and  $p_{1/2}$  states. Parity inversion ensues, with  $1/2^+$  and  $1/2^-$  at threshold. As a consequence the  $N = 8$  shell closure melts away,  $N = 6$  becoming a new magic number, testifying to the fact that large amplitude fluctuations can be, in nuclei, as important or even more important than static mean field effects. As a result  ${}^3_3\text{Li}_7$  is not bound. Adding one more neutron and switching on the bare pairing interaction (e.g. a contact force  $V(r_{12}) = -4\pi V_0 \delta(\mathbf{r}_1 - \mathbf{r}_2)$  with constant matrix element<sup>132</sup>  $G = 1.2 \text{ fm}^{-3} V_0 / A \approx (25/A) \text{ MeV}$ ), the screening  $r = \frac{(M_j)_{\text{halo}}}{(M_j)_{\text{core}}} \approx \frac{2}{2j+1} \left( \frac{R_0}{R} \right)^3 \approx 0.048$  (see Eq. (3.6.3)) resulting from the poor overlap between halo and core neutrons leads to a value of the strength of the pairing interaction  $(G)_{scr} = r \times G$  which is subcritical, and thus to an unbound system (see Sect. 3.6 and App. 3.B). In fact,  $G_{scr} = 0.048 \times 25/A \text{ MeV} \approx 0.1 \text{ MeV}$  and  $\Delta E = 2\bar{\epsilon}_{s_{1/2}} - G_{scr} \approx 0.3 \text{ MeV} - 0.1 \text{ MeV} \approx 0.2 \text{ MeV}$ . Summing up,

<sup>127</sup> Kanungo et al. (2015); Sackett et al. (1993); Zinser, M. et al. (1997)

<sup>128</sup> See Broglia et al. (2019) and references therein.

<sup>129</sup> See e.g. the corresponding discussion in Barranco et al. (2017).

<sup>130</sup> It is of notice that in discussing Fig. 2.9.1 use is made of the values calculated in NFT. This is also true in connection with the estimates carried out in Sect. 3.6.1.

<sup>131</sup> See Sect. 2.9.1.

<sup>132</sup> Brink, D. and Broglia (2005), pp 40-42. It is of notice that the difference with the number found in this reference  $G \approx 28/A \text{ MeV}$  is within the margin of uncertainties.

\* )  $\tilde{N} - \tilde{N}$  parte del mensaje (corregido)  
enviado a Vince

$G_{scr} < G_c$ ,  $G_c$  being the minimum value of the pairing coupling constant leading to a bound state<sup>133</sup>

*b) bold*

3) Considering the sloshing back and forth of the halo neutrons (with a small contribution from the core neutrons) against the core protons, leads to a dipole mode feeling a strongly screened repulsive symmetry potential. In keeping with the fact that  $\kappa_1^0 \sim 1/R^2$  ( $^{11}\text{Li}$ ), the screening factor can be estimated as  $((R/^{11}\text{Li})/\xi)^2$  ( $R = 4.58$  fm,  $\xi = 20$  fm,  $s \approx 0.052$ ), the value obtained in Sect. 3.6 being  $s = 0.043$ . In other words, while it takes a quantity proportional to  $5V_1 = 125$  MeV to separate protons from neutrons in the core, this price is reduced to  $s \times 5V_1 = 5.4$  MeV ( $(V_1)_{scr} = sV_1 \approx 1$  MeV) for halo neutrons. This is at the basis of the fact that  $\approx 8\%$  of the Thomas–Reiche–Kuhn sum rule (**input**) gets down to  $\lesssim 1$  MeV. Another way to say the same thing is that  $(V_1)_{scr} = sV_1$  is at the basis of the fact that the  $s_{1/2} - p_{1/2}$  energy difference ( $\Delta\tilde{\epsilon} \approx 0.45$  MeV) is only increased by a modest value ( $\hbar\omega_{pygmy} \approx 1$  MeV  $\approx 10^{21}$  Hz), while the  $E1$  single-particle strength remains essentially unchanged. Typical values in the case of nuclei lying along the stability valley being  $\approx 10^{-4}B_W(E1)$  for low-energy single-particle transitions, while in the present case one finds a value close to  $1B_W(E1)$ .

Now, the two halo neutrons dressed by the vibrations of the core (heavy arrowed lines in lowest left corner of Fig. 2.9.1) and interacting through the bare  $NN$ -pairing force are not bound. Consequently, the pygmy resonance will fade away almost as soon as it is generated (essentially lasting the neutron transversal time  $\approx 10^{-21}$  s). This, unless it is exchanged between the two neutrons forcing them to jump from the configuration  $s_{1/2}^2(0)$  at threshold ( $2 \times \tilde{\epsilon}_{s_{1/2}} \approx 0.3$  MeV) into  $p_{1/2}^2(0)$ , also close to threshold ( $2 \times \tilde{\epsilon}_{p_{1/2}} \approx 1.2$  MeV). In other words, one finds the dipole pygmy resonance acting as an intermediate boson which couples to the halo neutrons with a strength  $\Lambda \approx 0.5$  MeV (QRPA calculation). As a result, it contributes to the binding of the neutron halo Cooper pair with  $\approx 0.5$  MeV binding. Thus, the corresponding correlation energy  $E_{corr} \approx -0.3$  MeV is mainly due

<sup>133</sup> At the basis of superconductivity one finds the result obtained by Cooper (1956). He worked out the problem of two electrons interacting through an attractive interaction above a quiescent Fermi sea. Thus, all but two of the electrons are assumed to be noninteracting. The background of electrons enter the total problem only through the Pauli principle by blocking states below the Fermi surface from participating in the remaining two-particle problem. If one measures the kinetic energy  $\epsilon_k$  relative to its value at the Fermi surface only states with  $\epsilon_k > 0$  are available to the interacting pair of electrons. Cooper found that a bound state of the pair always exists for arbitrarily weak coupling so long as the potential is attractive near the Fermi surface, a mechanism which implies the instability of the normal phase, and found at the basis of superconductivity. Cooper pair binding is a rather remarkable result for the usual two-body problem. If one has only two particles coupled by an attractive interaction of finite range, they would not form bound states unless the attractive interaction exceeds a certain critical value, Cooper reduces the above 3-dimensional to a 1-dimensional quantal system (Gor'kov (2012)). Now, in  $^{11}\text{Li}$  the last two neutrons are very weakly bound. Consequently they move away from the neutron closed shell core  $^9\text{Li}$ , lowering in the process their relative momentum and forming a misty cloud or halo. One can thus view this system as the nuclear embodiment of a Cooper pair. The question then arises, why there is a critical value for the pairing interaction. The answer is spatial quantization, which is a three-dimensional feature, and is associated with the fact that the nucleus is a finite system.

to the dipole pygmy exchange process. The resulting symbiotic halo pair addition mode of  $^{11}\text{Li}$  can, in principle, be used as a building block of the nuclear spectrum, amenable to be moved around. A possible candidate for such a role is the first excited  $0^+$  state of  $^{12}\text{Be}$ , together with the associated dipole state built on it and eventually other fragments of the associated  $E1$ -low energy-strength.

To calculate the pygmy dipole resonance (PDR) of  $^{11}\text{Li}$  one needs to know the ground state of this nucleus (halo-pair addition mode) so as to be able to determine microscopically the occupation factors of the  $1s_{1/2}, 1p_{3/2}, \epsilon s_{1/2}, \epsilon p_{1/2}, \epsilon d_{5/2}, \dots$ , etc. states. This is the basic input needed to work out the corresponding QRPA equations, whose diagonalization provide the energy, transition density and probability of the mode. But to do so one is required to know the PDR. Arrived to this point, the protocol schematically presented in Fig. 2.9.1 implies to go back to 1 and repeat the whole procedure until convergence is achieved.

#### 2.9.4 $^{11}\text{Li}(p, p)^{11}\text{Li}$ optical potential and transfer reaction channels

NFT is based on elementary modes of excitation, modes which carry a large fraction of the nuclear correlation. Because its rules have no limitations concerning whether the excitations studied lie or not in the continuum, or whether the single-particle motion displays asymptotic conditions, it allows for a unified description of structure (s) and reactions (r) (NFT(s+r)). An example of the above statement is provided by Fig. 2.9.2. Graph (a) is a NFT-diagram describing one of the processes contributing to the elastic reaction  $^{11}\text{Li}(p, p)^{11}\text{Li}$  as the system propagates in time. This graph describes a polarization contribution to the global (mean field) optical potential describing proton elastic scattering off  $^{9}\text{Li}$ .

In what follows we describe the processes taking place in Fig. 2.9.2 (a) in the interval of time  $t_1 - t_{11}$ , starting from the  $t = -\infty$  situation in which a proton impinges on  $^{11}\text{Li}$ . At time  $t_1$ , the halo pair addition mode  $|0_v\rangle$  couples to a pure, bare configuration  $s_{1/2}^2(0)$ . At time  $t_2$ , and due to the zero point fluctuations associated with the quadrupole vibration of the  $^{11}\text{Li}$  core, the virtual state  $((p_{1/2}, p_{3/2}^{-1})_{2^+} \otimes 2^+)_{0^+}$  is created. At time  $t_4$ , one of the continuum  $s_{1/2}$  neutrons excites the quadrupole vibration of the core reabsorbing it at time  $t_6$ . As a result of this self energy process, its energy is lowered to threshold, becoming a virtual state. The other  $s_{1/2}$  continuum neutron state excites at  $t_3$  the PDR and moves into the  $p_{1/2}$  orbital after which, and due to Pauli principle, becomes exchanged with the homologous  $p_{1/2}$  of the  $(p_{1/2}, p_{3/2}^{-1})_{2^+}$  configuration, exchange process which is completed by time  $t_5$ . As a result the  $p_{1/2}$  state undergoes a conspicuous repulsion, becoming a resonant state. At time  $t_7$  the  $s_{1/2}$  neutron absorbs the PDR and moves into a  $p_{1/2}$  state. At time  $t_8$  it interacts, through the bare  $^1S_0$ -(pairing) interaction, with the other  $p_{1/2}$  neutron, completing the process by which the halo pair addition mode binds to the core  $^{11}\text{Li}$ . Before the two  $p_{1/2}$  neutrons couple to the  $|0_v\rangle$  state one of them is picked up at time  $t_9$  under the action of the proton-neutron interaction  $v_{np}$ , by the projectile (proton), to form a virtual deuteron. The recoil effect associated with the new mass partition being taken care of by the particle-recoil

a cartoon representation of a setup to measure one-nucleon transfer reactions is displayed. Also shown is a  $(NFT)_{ren}(s+r)$  diagram describing the process. In the **lower right** part of the figure, the lowest quasiparticle energy values are displayed as a function of  $\beta_2/(\beta_2)_0$  in comparison with the data. The root mean-square deviation between the experimental and theoretical levels as a function of a function of  $\beta_2/(\beta_2)_0$  and of  $G/G_0$  are shown in (e) and (f) respectively. In (g) the experimental energies of the members of the  $h_{11/2} \times 2^+$  multiplet shown in (d), are compared with the theoretical values calculated as a function of the ratio  $\beta_2/(\beta_2)_0$ . Finally in (h) the root mean-square deviation between the experimental and theoretical energies of the members of the  $h_{11/2} \times 2^+$  multiplet shown in (g) are given as a function of  $\beta_2/(\beta_2)_0$ .

Summing up, the nuclear structure landscape is well funneled and theory provides an overall account of the data, when the physical values of  $\beta_2$ ,  $G$  and  $m_k$  are used.

## 2.11 Summary

In Fig. 2.10.1 the results of a “complete”  $(NFT)_{ren}(r+s)$  description of the open shell superfluid nucleus  $^{120}\text{Sn}$  in terms of the  $^{120}\text{Sn}(p,t)^{118}\text{Sn(gs)}$ ,  $^{122}\text{Sn}(p,t)^{120}\text{Sn(gs)}$ ,  $^{120}\text{Sn}(p,d)^{119}\text{Sn}$ ,  $^{121}\text{Sn}(p,d)^{120}\text{Sn}$ ,  $^{119}\text{Sn}(\alpha, \alpha')^{119}\text{Sn}$  ( $\gamma$ -decay) cross sections, energies and transition probabilities are displayed in comparison with the experimental findings. Arbitrarily forcing the particle-vibration coupling (PVC) strength, the strength of the bare pairing force and the value of the  $k$ -mass to depart from their “physical” values, one can test the robustness of the  $NFT(r+s)$  picture of  $^{120}\text{Sn}$  given, and of the well funneled character of the associated nuclear structure and reaction landscape.

*In a very real sense this, namely the results collected in Fig. 2.10.1 is a nucleus<sup>141</sup>. That is, the summed experimental and theoretical structural information accessed through asymptotic states,<sup>\*</sup> outcome of simultaneously probing the system with a complete array of experiments (elastic, anelastic and associated  $\gamma$ -decay, as well as one- and two-nucleon transfer reactions), and of calculating the corresponding observables with an equally ample array of theoretical tools, as provided by  $(NFT)_{ren}(r+s)$ .*

## Appendix 2.A Inelastic Scattering

In this Appendix we briefly discuss how to extract values of the effective deformation parameter  $\beta_L$  from inelastic scattering absolute differential cross sections in the most simple and straightforward way, ignoring all the complications associated with the spin carried by the particles, the spin-orbit dependence of the

<sup>141</sup>For details, see Idini et al. (2015), and Broglia et al. (2016), see also Fig. 2.4.1.

\*<sup>142</sup>) Another examples being provided by the result displayed in Fig. 2.9.1 concerning  $^{11}\text{Li}$  and Fig. 7.3.1 regarding  $^{11}\text{Be}$  (see also sect. 7.6.2).